Disuse-induced Preferential Loss of the Giant Protein Titin Depresses Muscle Performance via Abnormal Sarcomeric Organization

Jun Udaka,[1] Shintaro Ohmori,[2] Takako Terui,[1] Iwao Ohtsuki,[1] Shin'ichi Ishiwata,[2] Satoshi Kurihara,[1] and Norio Fukuda[1]

[1]Department of Cell Physiology, The Jikei University School of Medicine, Tokyo 105-8461, Japan
[2]Department of Physics, Waseda University, Tokyo 169-8555, Japan

Persistent muscle weakness due to disuse-associated skeletal muscle atrophy limits the quality of life for patients with various diseases and individuals who are confined to bed. Fibers from disused muscle exhibit a marked reduction in active force production, which can exacerbate motor function, coupled with the well-known loss of muscle quantity. Despite recent understanding of the signaling pathways leading to the quantity loss, the molecular mechanisms of the depressed qualitative performance still remain elusive. Here we show that long-term disuse causes preferential loss of the giant sarcomere protein titin, associated with changes in physiologic muscle function. Ca^{2+} sensitivity of active force decreased following 6 wk of hindlimb immobilization in the soleus muscle of the rat, accompanied by a shift in the length-active force relationship to the shorter length side. Our analyses revealed marked changes in the disused sarcomere, with shortening of thick and thin filaments responsible for altered length dependence and expansion of interfilament lattice spacing leading to a reduction in Ca^{2+} sensitivity. These results provide a novel view that disuse-induced preferential titin loss results in altered muscle function via abnormal sarcomeric organization.

The Journal of General Physiology

INTRODUCTION

Disuse atrophy is caused by muscular inactivity, and is characterized by a reduction in muscle protein levels, as well as by a decrease in active force production. Recent advances in cell and molecular biology technology have enabled identification of multiple triggering factors for the protein loss associated with weightlessness (for reviews see Glass, 2003; Jackman and Kandarian, 2004; Lynch et al., 2006). Likewise, there is solid evidence that the disused sarcomere exhibits a marked decrease in active force production, including a fall in Ca^{2+} sensitivity as well as a reduction in active force per fiber cross-sectional area (e.g., Fitts et al., 2000); however, the molecular mechanisms are still poorly understood. The depressed performance likely exacerbates muscle weakness. The giant elastic protein titin (connectin) spans the distance from the Z-line to the M-line in the striated muscle sarcomere and serves as a molecular ruler for self-assembly of sarcomere proteins during myofibrillogenesis, as well as a passive force generator (e.g., Whiting et al., 1989; Trinick, 1994; Gregorio et al., 1999; Granzier and Labeit, 2004). In the present study, we tested the hypothesis that the depressed muscle performance results from abnormal sarcomeric organization, caused by changes in titin expression, using a long-term hindlimb immobilization model in the rat.

Correspondence to Jun Udaka: judk@jikei.ac.jp; or Norio Fukuda: noriof@jikei.ac.jp

MATERIALS AND METHODS

Disuse Atrophy Model and Single Fiber Mechanics

Male Wistar rats (300−330 g) were used. All experiments performed in the present study conform to the Guide for the Care and Use of Laboratory Animals (1996. National Academy of Sciences, Washington D.C.). Hindlimb immobilization was performed based on a previous report (St-Amand et al., 2001). In brief, under anesthesia with pentobarbital sodium (50 mg/kg I.P.), the left leg was immobilized with casting tape (type 82002-J, Sumitomo 3M; changed every week) to keep the ankle joint in a fully extended position. No intervention was performed on the right leg (control). After 6 wk of immobilization, animals were anesthetized with pentobarbital sodium (50 mg/kg I.P.), and the whole soleus muscles were dissected from both legs and quickly immersed in oxygenated Ca^{2+}-free Tyrode's solution (for composition see Fukuda et al., 2001b) containing 30 mM 2,3-butanedione monoxime (BDM) at 30°C. We used the antigravity soleus muscle throughout the study, because of its high susceptibility to disuse (see Fitts et al., 2000). The extensor digitorum longus (EDL) muscle was dissected from the leg with no immobilization. No reduction of body weight was observed during immobilization (unpublished data). Rabbit psoas muscle was obtained from white rabbits. Small bundles (1−2 mm diameter; ~10 mm length) were dissected from the muscles and skinned in relaxing solution (5 mM MgATP, 40 mM BES, 1 mM Mg^{2+}, 10 mM EGTA, 1 mM dithiothreitol, 15 mM phosphocreatine, 15 U/ml creatine phosphokinase, 180 mM ionic strength, adjusted by K-propionate, pH 7.0)

Abbreviations used in this paper: BDM, 2,3-butanedione monoxime; Dx, dextran T-500; EDL, extensor digitorum longus; MHC, myosin heavy chain; MyBP-C, myosin-binding protein C; PF, passive force; SL, sarcomere length.

containing 1% (wt/vol) Triton X-100 and 10 mM BDM overnight at ~3°C. Overnight treatment with Triton X-100 may result in loss of some structural proteins, in addition to cytoplasmic proteins; however, this was needed to almost completely remove membrane-based proteins, without any significant effect on the active and passive properties of control and disused fibers (unpublished data; see Fukuda et al., 2003, 2005). The preparations were then washed thoroughly with relaxing solution and stored for up to 2 d in relaxing solution at ~3°C. To prevent protein degradation, all solutions contained protease inhibitors: PMSF (0.5 mM), leupeptin (0.04 mM), and E64 (0.01 mM). Active force was measured with a single fiber, based on our previous studies (Fukuda et al., 2000, 2001a,b; pCa adjusted by Ca/EGTA). Sarcomere length (SL) was measured by laser diffraction and adjusted to 2.4 μm during relaxation. For the measurement of Ca^{2+} sensitivity of active force, $[Ca^{2+}]$ was varied from pCa 7.0 to 4.5. The curves were fitted to the Hill equation and the values of pCa_{50} (midpoint of the force–pCa curve) and n_H (Hill coefficient) were obtained. Rigor cross-bridge–based active force was produced by lowering [MgATP] from pMgATP (= −log [MgATP]) 5.0 to 6.5 in the absence of Ca^{2+}, and $pMgATP_{50}$ (midpoint of the curve) and n_H were obtained (Mio et al., 2002).

Passive force (PF) was measured based on our previous study (Fukuda et al., 2001a), starting from SL 2.2 μm. In brief, a single fiber was stretched at a constant velocity of 0.1 muscle length per second and then held for 1 min, followed by a stretch to a longer SL (force measured at 2.4, 2.6, 2.8, 3.0, 3.4, and 3.8 μm in this order). Quasi-steady-state PF was measured at each SL, and titin-based PF was obtained as total PF minus residual PF after the KCl/KI treatment (Fukuda et al., 2003). The average PF data were analyzed with an exponential function, i.e., $PF = A \times \exp(k \times (SL - SL_0)) - 1$, where A is the amplitude, k is the exponent of PF, and SL_0 is the intercept on the SL axis, i.e., the zero load SL (set at 2.2 μm due to zero passive force).

To obtain the SL–active force relationship, a single fiber was activated at pCa 4.5 at each SL (see above), 1 min after stretch. SL was increased after the solution had been changed to relaxing solution. Active force was plotted as compared with the maximum (at SL 2.4 or 2.6 μm), before stretch. The active force data were fitted to a three polynomial function of the type: active force = $y_0 + a \times SL + b \times SL^2 + c \times SL^3$, where y_0 is the offset and a, b, and c are the coefficients. SL_{50} (midpoint of the descending limb) was obtained as an index of length dependency.

Fiber width (diameter) was determined at three or four points along each fiber, and calculated from the mean width of these measurements, with the assumption that the fiber forms a cylindrical cross section. All mechanical studies were conducted at 15°C.

Electron Microscopy

Intact or skinned fibers were used based on our previous study (Fujita et al., 1996). After measuring SL by laser diffraction during relaxation, solution was replaced with a fixation solution containing 2% (vol/vol) glutaraldehyde. Longitudinal sections as well as cross sections were cut (~40 nm thickness) and observed with an electron microscope (H-7500, Hitachi Co.). NIH image software was used to quantify the average thick filament length. Since the clarity was not sufficiently high in the electron micrographs of intact preparations, due presumably to the presence of intracellular components, we used skinned sarcomeres to quantitatively analyze the average thick filament length.

Fluorescence Measurement of A-band Width and I-Z-I Brush Width

To measure the A-band width, specific labeling of myosin heavy chain (MHC) was performed based on our earlier work (Ishiwata et al., 1987). In brief, skinned single fibers were bathed in relaxing solution containing 1 μM tetramethyl rhodamine-5-maleimide (Molecular Probes) for 30 min at 4°C. The average A-band width was quantified with NIH image software, under a laser scanning confocal microscope system (LSM-CG200, Olympus Co.). To measure the I-Z-I brush width, skinned single fibers were immersed in relaxing solution containing 1 μg/ml Alexa488-phalloidin (Molecular Probes) at 3°C for 3 h (Yasuda et al., 1994). The I-Z-I brush width was quantified with NIH image software, under the confocal microscope system.

Gel Electrophoresis

Various acrylamide gels (2−7% titin, 8%, and 15%) were stained with Coomassie brilliant blue, and the optical density (OD) of band of interest was determined using One-D-Scan (v. 2.03, Scanalytics Co.) (Fukuda et al., 2003, 2005). Proteins were identified by comigration with known standards. In some experiments, a range of loadings (4−16 μl) was electrophoresed on the same gel, allowing us to determine integrated OD-loading relations. The slope of the linear range of integrated OD versus loading was obtained from linear regression analysis. The slope ratio for samples from control versus disused soleus muscles was then calculated. Protein concentration was measured by BCA Protein Assay Kit (Pierce Chemical Co.).

Interfilament Lattice Spacing Measurement

Interfilament lattice spacing was measured based on a previous study (Higuchi and Umazume, 1986). In brief, skinned single fibers were held vertically in a chamber with a capacity of 0.09 ml solution, and SL was adjusted to 2.4 μm during relaxation by monitoring the laser diffraction. The chamber was perfused with relaxing solution containing 30 mM BDM, at a rate of 0.4 ml/min (15°C). The positions of the 1,0 reflections were measured by NIH image software to obtain the $d_{1,0}$ value.

Statistics

Significant differences were assigned using the paired or unpaired Student's *t* test (as appropriate). NS denotes insignificant. Linear regression analysis was used to test correlations between parameters. In all cases, statistical significance was verified with the P value less than 0.05 (*$P < 0.05$). All data were expressed as mean ± SEM, with *n* representing the number of experiments.

RESULTS AND DISCUSSION

First, we demonstrated the macroscopic and microscopic changes in muscle morphology after disuse; Fig. 1 A compares soleus muscles taken from control and immobilized legs, from the same animal. We observed marked reductions in size and wet weight of muscle (176.0 ± 4.7 vs. 115.7 ± 4.4 mg; $P < 0.05$, $n = 35$), hence confirming it to be a suitable model for structural and mechanical analyses. We observed isoform switching of MHC upon disuse, i.e., a decrease in MHC I (slow type) with a concomitant increase in MHC IIB (fast type) (see Fitts et al., 2000).

We then conducted electron microscopy studies with intact muscles (Fig. 1 B). Myofibrils were thinner in disused muscle than in healthy muscle, as is commonly known (e.g., Riley et al., 2000). In addition, the A/I junction was found to be indistinct in disused muscle, with the visible M-line preserved. Glycogen-like granules were similar in both muscles; however, upon disuse, the mitochondrial regularity disappeared, and the number of small granule vesicles increased.

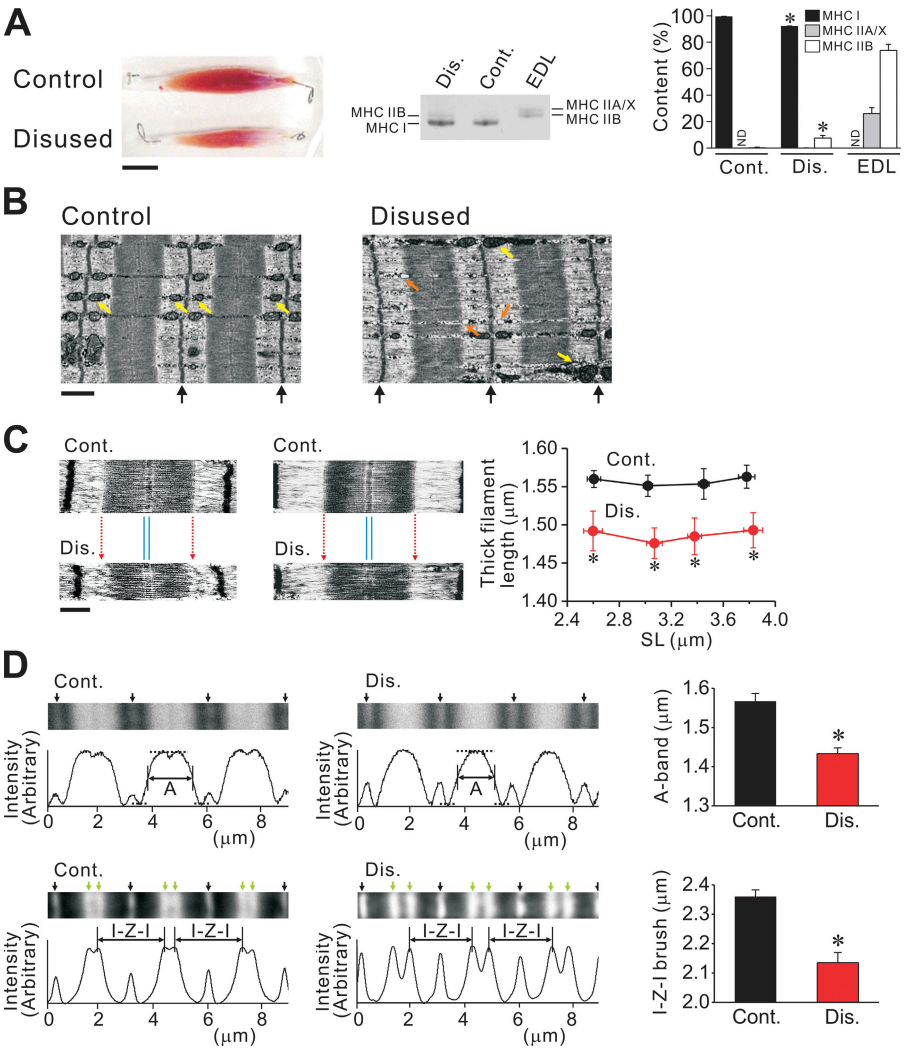

Figure 1. Disuse-induced morphological changes in muscle. (A) Changes in muscle size (left) and MHC expression (middle and right). Bar, 1 cm. Same animal was used in left and middle figures. Muscle bundles (~30 mg) were solubilized and run for gel electrophoresis. EDL muscle was used as control for separation of MHC IIA/X and IIB. Cont., control without disuse; Dis., disused. MHC was run on 8% gel. In bar graph, ND indicates "not detectable" for densitometric analysis. *, $P < 0.05$, compared with the corresponding value for control soleus muscle. (B) Electron micrographs of longitudinal sections of intact soleus muscle, with (right) and without (left) disuse (taken from the same animal). SL ~ 3.2 μm. Black arrows indicate the positions of the Z-line. Bar, 1 μm. Yellow arrows indicate mitochondria. Orange arrows indicate small granule vesicles. (C) Electron micrographs of longitudinal sections of sarcomeres in skinned single fibers, with (bottom) and without (top) disuse. Images at short (~2.6 μm; type I) and long (~3.2 μm; type I/II) SLs are shown (same animal used for each SL). Red dotted arrows indicate the position of the A/I junction in control sarcomere. Note similar thickness of the M-line in control and disused sarcomeres (indicated by thin blue lines) (see Fig. 4 B). Bar, 0.5 μm. Graph shows average thick filament length in control vs. disused fibers at various SLs (from eight animals; type I and I/II fibers pooled for disused group). *, $P < 0.05$, compared with control. (D) Fluorescence analyses of sarcomeres in skinned fibers, with and without disuse. Typical images and corresponding intensity profiles are shown. Top, A-band width measurement. Images: black arrows indicate the positions of the Z-line. Intensity profiles: horizontal dashed lines indicate the highest and lowest intensity values and vertical lines the midpoint of fluorescent intensity. The distance between vertical lines was defined as the average A-band width (noted as A). Bar graph summarizes the data from four animals ($n = 10$; type I and I/II fibers pooled for disused group). SL was 2.70 ± 0.07 and 2.78 ± 0.08 ($P > 0.05$) in control and disused muscle, respectively. Bottom, I-Z-I brush width measurement. Images: black arrows indicate the positions of the Z-line and green arrows the positions of the pointed end of the thin filament (Yasuda et al., 1994). The thin filament length was obtained by dividing the I-Z-I brush width (noted as I-Z-I) by a factor of 2. Bar graph summarizes the data from four animals ($n = 6$; type I and I/II fibers pooled for disused group). The value of the thin filament length in control muscle was similar to that reported previously with electron microscopy (Herzog et al., 1992). SL was 2.86 ± 0.05 and 2.73 ± 0.03 ($P > 0.05$) in control and disused muscle, respectively. *, $P < 0.05$.

Using skinned single fibers, we found that the thick filament length was not uniform in the disused sarcomere, with shorter filaments coexisting with normal-length filaments, resulting in shortening of the average thick filament length, over the range of SL up to ~3.8 μm (by ~0.07 μm; measured by electron microscopy) (Fig. 1 C). The coexistence of thick filaments with varying lengths can account for the indistinctive A/I junction observed in the intact disused muscle preparation (Fig. 1 B). The disuse-induced shortening of thick filaments was observed in fibers expressing solely MHC I (type I) as well as in fibers expressing both MHC I and II (type I/II).

Fig. 1 D shows fluorescence analyses for the lengths of thick and thin filaments in control vs. disused muscles. We found that the A-band width (i.e., average thick filament length) was significantly less in disused muscle (i.e., by ~0.1 μm; Fig. 1 D, top), to a magnitude similar to that detected by electron microscopy. Earlier electron microscopy studies revealed, on the other hand, that disuse decreases thin filament density and length in human soleus muscle after spaceflight (Riley et al., 2000) and after bed rest (Riley et al., 1998). The present study quantified the change in the average thin filament length, in that it was shorter by ~0.1 μm after disuse (1.07 ± 0.02 vs. 1.18 ± 0.01 μm; $P < 0.05$) (expressed as I-Z-I

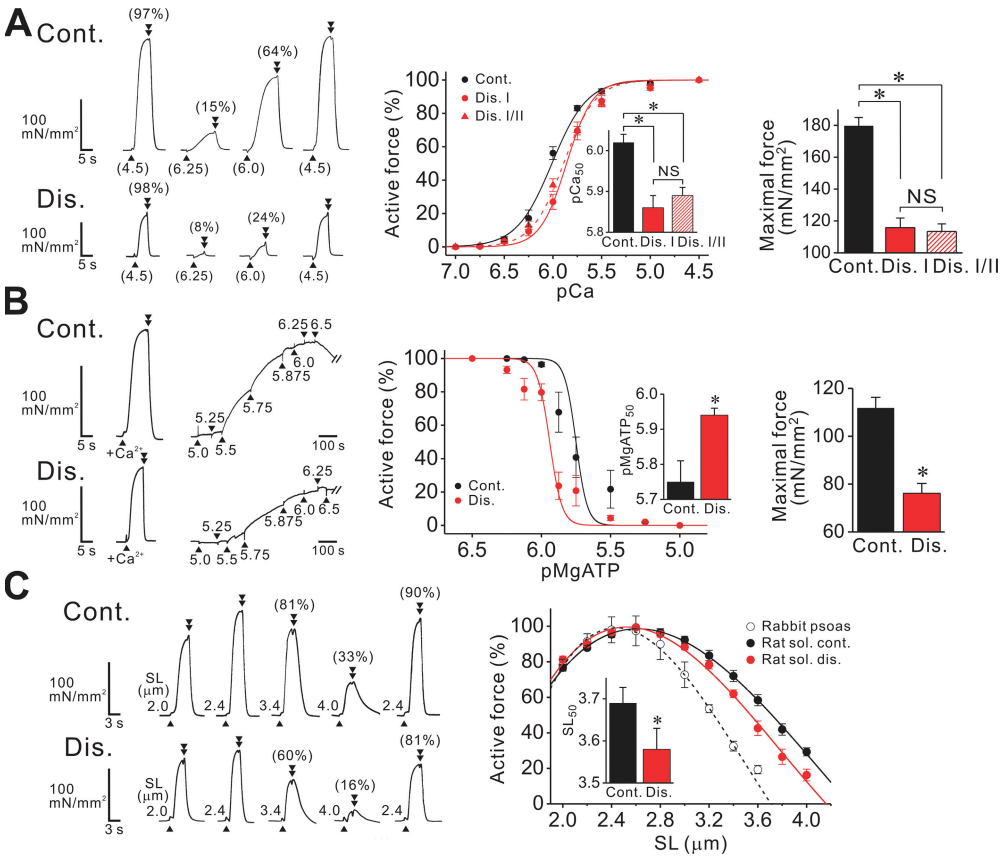

Figure 2. Disuse-induced changes in mechanical properties of single fibers. (A) Ca^{2+}-activated force. SL 2.4 μm. Left, chart recording for fibers with (bottom) and without (top) disuse (both type I fibers), taken from the same animal. Numbers in parentheses at the bottom indicate pCa. Arrowheads and double arrowheads indicate the points at which solution was switched from relaxation to contraction and from contraction to relaxation, respectively. Numbers in parentheses on top of force records indicate the percentage compared with the maximum obtained at the end of experiment. Middle, force–pCa curves, normalized at pCa 4.5. In disuse, solid and dashed lines indicate type I and I/II fibers, respectively. Inset, pCa_{50}. n_H: 2.39 ± 0.16 in control fibers, and 3.21 ± 0.47 and 2.67 ± 0.30 in disused type I and I/II fibers, respectively. Right, maximal Ca^{2+}-activated force, obtained at pCa 4.5. $n = 8-10$ (three animals). *, $P < 0.05$. (B) Ca^{2+}-independent rigor cross-bridge–based activation. Left, chart recording for fibers with (bottom) and without (top) disuse (taken from the same animal). Numbers indicate pMgATP. Middle, force–pMgATP curves (normalized at pMgATP 6.25 and 6.5 for control and disuse, respectively). Inset, $pMgATP_{50}$. n_H: 10.64 ± 2.09 and 9.81 ± 1.74 in control and disused fibers, respectively. Right, maximal rigor cross-bridge–based active force. Type I fibers were used for both groups. $n = 8$ (two animals). *, $P < 0.05$. (C) SL dependence of active force, measured at pCa 4.5. Left, chart recording comparing active forces in control and disused fibers at various SLs (taken from the same animal). Numbers in parentheses indicate active force compared with the maximum obtained at SL 2.4 μm before stretch. Rightmost record, active force at SL 2.4 μm obtained after stretch. Right, SL–active force relationship in control and disused fibers (dotted line, rabbit psoas muscle). Maximal force at SL 2.4 or 2.6 μm: 215.5 ± 22.0 and 153.4 ± 13.4 mN/mm² ($P < 0.05$), respectively, in control and disused fibers of rat soleus muscle (240.7 ± 15 mN/mm² in rabbit psoas muscle). Inset, SL_{50} (intercept on the SL axis) in control vs. disused fibers of rat soleus muscle. Control fibers: y0, a, b, and c were −473.5 ± 68.3, 517.4 ± 77.0, −144.8 ± 28.2, and 11.7 ± 3.3, respectively. Disused fibers: −596.2 ± 77.6, 661.4 ± 80.5, −196.5 ± 27.1, and 17.3 ± 2.9, respectively. Type I and I/II fibers were pooled for the disused group. $n = 8$ (four animals). *, $P < 0.05$.

brush width in Fig. 1 D, bottom). Therefore, disuse brings about both quantitative decrease in muscle size and qualitative change in sarcomeric ultrastructure.

We then analyzed the effects of disuse on steady-state active force at the slack SL (2.4 μm), by dividing skinned single fibers into two groups, i.e., fiber type I and I/II groups, depending on MHC expression. It was found that Ca^{2+} sensitivity was lower in disused fibers in both groups, accompanied by a reduction in maximal Ca^{2+}-activated force (Fig. 2 A). Disuse did not significantly change n_H (see legend). Due to similar Ca^{2+} sensitivity in disused type I and I/II fibers, we disregarded the differences in MHC expression in the following experiments.

To test whether the disuse-induced reduction in active force is modulated at the cross-bridge level, rather than by altering the process of Ca^{2+} binding to troponin C, we compared Ca^{2+}-independent rigor cross-bridge–based active force in control vs. disused fibers. We found that the force–pMgATP curve was shifted leftward upon disuse, with a reduction in maximal Ca^{2+}-independent active force, indicating that active force generation is suppressed at the cross-bridge level (Fig. 2 B). Therefore, regardless of the activator, either Ca^{2+} or cross-bridges, depression of the active force production in disused fibers indicates that a smaller fraction of cross-bridges is formed in the sarcomere, at a given level of thin filament activation.

Considering the finding that thick and thin filaments become shorter upon disuse (Fig. 1, C and D), the length dependence of active force is likely to be altered accordingly. Expectedly, we found a significant change in the relationship upon disuse, in that the descending limb of the relationship was shifted leftward, with no significant change in the ascending limb (Fig. 2 C). This result

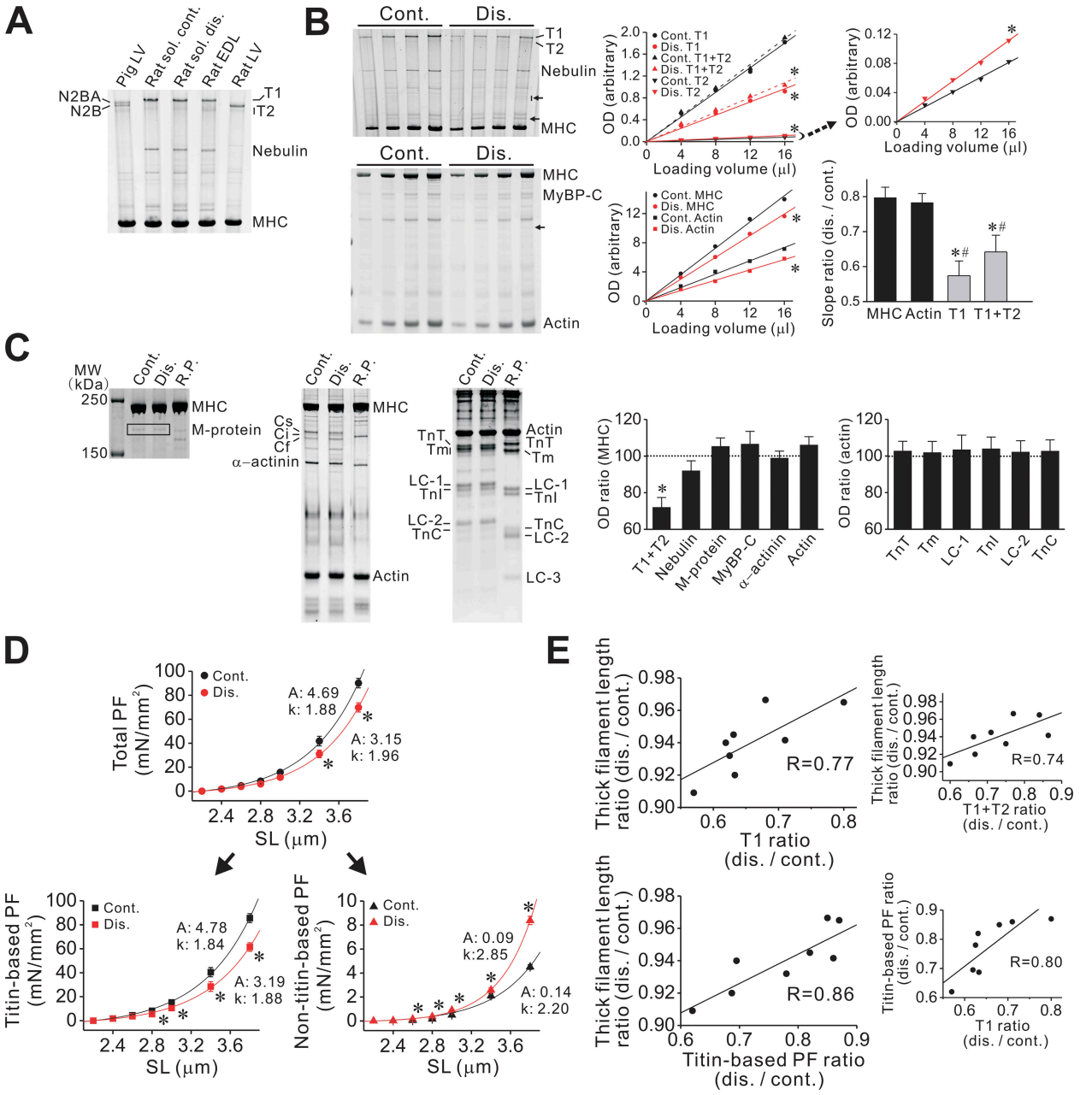

Figure 3. Disuse-induced changes in sarcomere protein expressions. (A) Titin expression in soleus (with and without disuse) and EDL muscles of the rat (all from the same animal). N2BA and N2B titins from skinned left ventricular muscles (LV) of the rat and pig are shown as known standards for molecular weight (Fukuda et al., 2003, 2005). T1, intact titin in soleus (and EDL) muscles. T2, titin's degradation product(s). (B) Effect of disuse on titin level, as compared with MHC and actin levels. Intact rat soleus muscle preparations, with and without disuse, were solubilized (0.25 mg/ml total protein) and electrophoresed with varying loading volumes (4, 8, 12, and 16 μl). Left, gels showing changes in titin (top) and MHC and actin (bottom) (control and disused muscles were taken from the same animal). Small arrows indicate protein bands that increased in intensity in disuse. MyBP-C, myosin-binding protein C. Middle, relationship between loading volume and OD for titin (top) as well as for MHC and actin (bottom). Top, T1 (solid lines) and T1+T2 (dashed lines). The relationship for T2 is shown on right with a larger scale, with the average slope ratio of 1.49 ± 0.18 (disused vs. control). Asterisks indicate slope significantly different ($P < 0.05$) compared with corresponding control. R values for the regression lines: 0.98–0.99. Bar graph, summary showing slope difference ratio, disuse vs. control. Upon disuse, titin (both T1 and T1+T2) was decreased to a magnitude greater than MHC (*, $P < 0.05$) or actin (#, $P < 0.05$). Eight animals were used. (C) Analyses of major sarcomere proteins, i.e., M-protein (left gel; 8%), MyBP-C, α-actinin, actin (middle gel, 8%), troponin T (TnT), tropomyosin (Tm), myosin light chain 1 (LC-1), troponin I (TnI), myosin light chain 2 (LC-2), troponin C (TnC), and myosin light chain 3 (LC-3) (right gel, 15%). R.P., rabbit psoas muscle. Data were taken from skinned muscles, except for titin and nebulin (data insignificant as compared with those obtained with intact muscles; not depicted). Bar graphs show disused-induced changes in the level of major sarcomere proteins, normalized with MHC or actin, depending on the molecular weight. *, $P < 0.05$ with Tukey's multiple comparison. Eight animals were used. (D) PF in skinned single fibers. The exponential parameters are shown in figure, with titin-based and nontitin-based PF separated based on KCl/KI treatment.

provides an important physiological implication that disuse-induced active force depressions depend on SL, namely, greater in the long SL range. Taken together, cross-bridge formation is reduced in disused muscle, accompanied by a change in the length dependence.

Given titin's role as a molecular ruler (Whiting et al., 1989; Trinick, 1994; Gregorio et al., 1999), the abnormalities in the sarcomeric structure in disused muscle (Fig. 1, B–D) may be due to a change in its expression, resulting in depressed mechanical properties (Fig. 2, A–C). As shown in Fig. 3 A, molecular weight changes were not observed for titin in disused muscle. Instead, our analysis revealed its marked preferential loss (Fig. 3 B); the level of actin and myosin was decreased by ~20% after disuse in intact muscle, while the magnitude was more pronounced for titin, with the value of ~45% (hence resulting in a reduction in the ratio of titin to MHC; see Fig. 3 C). Also, degradation was elevated for titin, as shown by an increase in the level of its degradation product(s) (T2) (Fig. 3 B). In other studies, titin loss was also observed after hindlimb suspension in rats, but with no clear degradation, after unloading for 2 wk (Toursel et al., 2002), but not for 3 d (Goto et al., 2003). It can therefore be said that it is a universal phenomenon associated with long-term muscle wasting.

The examination of the expression profiles of other major sarcomere proteins revealed no significant preferential changes in any protein tested, other than titin (Fig. 3 C). When OD was normalized with that of MHC or actin, depending on the molecular weight, only titin was found to be significantly reduced (Fig. 3 C, bar graphs on the right). Therefore, proteins are reduced disproportionately in long-term disuse, with the effect on titin largest among the major sarcomere proteins.

In skeletal muscle, at least half of total protein is thick and thin filament based, and this fraction is lost at a faster rate than other muscle proteins in disuse (Jackman and Kandarian, 2004). The increase in the intensity of some bands in disused muscle (Fig. 3 B, arrows) indicates that the expression of nonsarcomere (or minor/unknown sarcomere) proteins may increase relative to that of the major sarcomere proteins tested in the present study.

It has been reported that gene expression is reduced for nebulin in disuse (St-Amand et al., 2001). In the present study, the level of nebulin showed an appreciable decrease in some animals (as in Fig. 3 B), but the result was not statistically significant for an average of eight animals. Considering a possible role of nebulin as a ruler for thin filament formation (Littlefield and Fowler, 1998), a slight reduction in its protein level may in part be responsible for the shortening of thin filaments (Fig. 1 D) (Riley et al., 1998, 2000). We also observed isoform switching of myosin-binding protein C (MyBP-C), from the slow type (Cs) to the fast type (Cf) as well as to the intermediate type (Ci) (Fig. 3 C; see McCormick et al., 1994; St-Amand et al., 2001). However, the total MyBP-C level was not significantly reduced in disuse (Fig. 3 C).

No study has directly examined whether titin indeed regulates thick filament formation in vivo, because of embryonic lethality. However, a study by van der Ven et al. (2000) clearly demonstrated that a functional knockout of titin results in defective thick filament formation in a cell culture model. Therefore, it is reasonable to consider that larger reduction of this protein compared with myosin and, presumably, MyBP-C results in abnormal thick filament formation during myofibrillogenesis in vivo. Reportedly, there are approximately six titins per half-thick filament (Granzier and Irving, 1995). Therefore, an ~30% preferential reduction in disuse (Fig. 3 C) will reduce the number from approximately six to approximately four, which may cause abnormal myosin polymerization, due to a lack of thick filament length regulation. The reduction of the thin filament length in disuse (Fig. 1 D) may also occur secondary to the thick filament shortening, independent of nebulin loss, because the myosin/titin array reportedly determines the thin filament length by positioning the thin filament pointed end, relative to the Z line, thereby indirectly regulating the thin filament length (Littlefield and Fowler, 1998).

It is well established that both protein synthesis and breakdown rates are altered in disuse atrophy and play a role in muscle protein loss (Glass, 2003; Jackman and Kandarian, 2004). The increase in T2 (Fig. 3 B) indicates that elevated proteolysis (such as by calpains; see Jackman and Kandarian, 2004) leads at least in part to a decrease in the titin level, apparently to a magnitude greater than for other proteins, due to the relative proteolytic sensibility of titin's PEVK segment in the I-band (Helmes et al., 1996). However, considering the observation that not only intact titin (T1) but total titin (T1+T2) was less than MHC or actin in disuse (Fig. 3 B, bar graph), it is unlikely that proteolysis alone can fully

Type I and I/II fibers pooled for the disused group. $n = 10$ (four animals). *, $P < 0.05$ compared with control. (E) Relation between thick filament length ratio and titin (T1) ratio (top; thick filament length ratio vs. T1+T2 ratio shown on right) or titin-based PF ratio (bottom, titin-based PF ratio vs. T1 ratio shown on right). The average thick filament length was measured in randomly chosen 20 sarcomeres in one fiber with electron microscopy, and the ratio was obtained by comparing the average values from six fibers, with or without disuse, for one animal. Titin level ratio was obtained by comparing the slopes in B, disused vs. control. Titin-based PF was obtained at SL 3.8 μm, 1 min after stretch, from six fibers, with or without disuse, and the ratio was obtained by comparing the average values, for one animal. Type I and I/II fibers were pooled for the analyses of the disused group. Data from eight animals are shown for each relationship. Significant correlations were obtained as $P < 0.05$ in all figures.

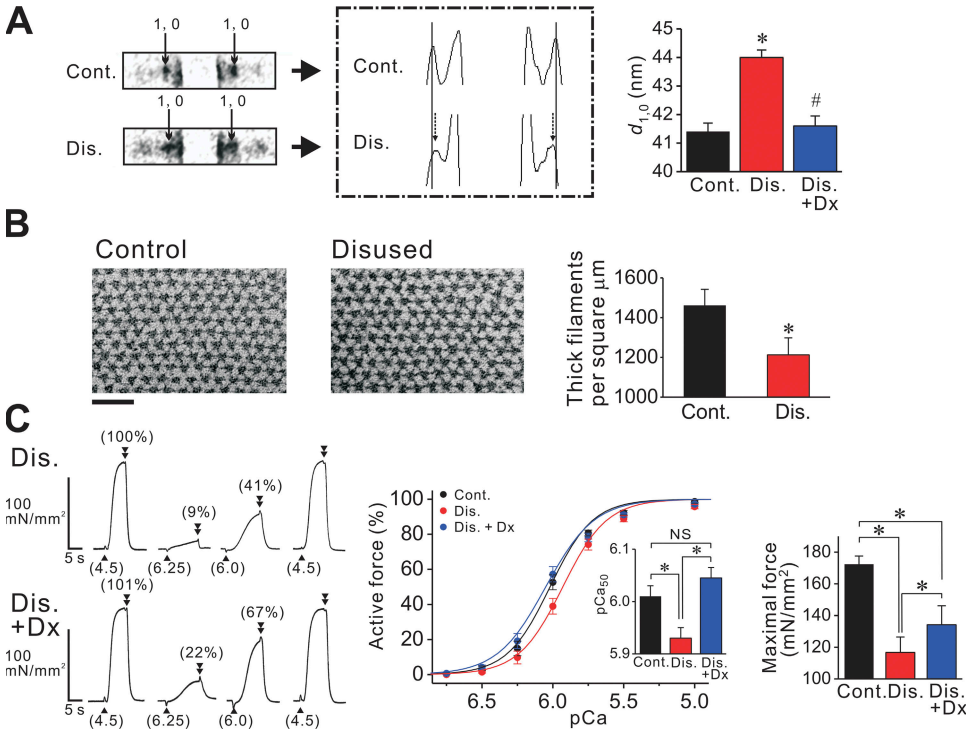

Figure 4. Interfilament lattice spacing measurement. (A) Left, X-ray patterns from skinned single fibers, with and without disuse, showing 1,0 spots, as indicated by small arrows (fibers were taken from the same animal). SL 2.4 µm. Middle, densitometric analysis of the left figure. Thin lines indicate the positions of 1,0 spots in control. Note inward shift of 1,0 spots upon disuse, as shown by small dashed arrows. Right, summary of $d_{1,0}$ values from eight animals. Dx 2% (wt/vol) was applied on disused fibers. *, $P < 0.05$ (or #, $P < 0.05$) compared with control (or disused) fibers. Type I and I/II fibers pooled for the disused group. (B) Thick filament density measurement with electron microscopy. Left, cross-sectional electron micrographs of single skinned fibers from control and disused muscles, at (near) the M-line (SL ~ 3.0 µm). Right, summary of thick filament density in control and disused fibers. Type I and I/II fibers were pooled for the analyses of disused fibers. $n = 15$ (5 animals). *, $P < 0.05$. (C) Active force measurement testing the effect of lattice shrinkage by Dx in disused single fibers. Left, typical chart recording showing the effect of 2% (wt/vol) Dx on active force (same disused fiber used throughout experiment). Numbers in parentheses at the bottom indicate pCa and those on top of force records indicate the percentage compared with the maximum obtained at the end of experiment. Middle, force–pCa curves. All curves were normalized at pCa 4.5. Inset, pCa_{50}. nH: 2.87 ± 0.27 in control fibers, and 2.79 ± 0.11 and 2.54 ± 0.18, respectively, in the absence and presence of Dx in disused fibers. Right, summary of maximal Ca^{2+}-activated force. Type I and I/II fibers were pooled. $n = 8-10$ (four animals). *, $P < 0.05$.

account for the observed titin loss. We therefore consider that in long-term disuse, preferential titin loss is caused synergistically by both elevated proteolysis (and/or ubiquitination) and reduced synthesis.

As expected, PF, especially titin-based PF, decreased in single fibers from disused muscle, with a concomitant increase in nontitin-based PF (Fig. 3 D). However, the shorter thick filaments may give an increase in PF due to increased strain of extensible I-band region of titin. A significant correlation between titin (T1) level and titin-based PF (Fig. 3 E, bottom right) strongly indicates that the decrease in titin-based PF results from preferential titin loss. We then investigated the role of titin loss in the formation of abnormal sarcomere structure, by comparing the titin level (or passive force) and the thick filament length in individual animals. As shown in Fig. 3 E, we found a significant coupling of the average thick filament length with titin level (for both T1 and T1+T2) (top) and with titin-based PF (bottom); that is, the A-band disruption was enhanced with titin loss. These positive correlations led us to propose that preferential titin loss is the primary cause of the abnormal sarcomeric structure in disuse atrophy.

Several recent lines of evidence strongly indicate that the lateral separation of thick and thin filaments, primarily regulated by titin as a lattice stabilizer via its passive force, affects the likelihood of myosin attaching to the thin filament in the striated sarcomere (Cazorla et al., 2001; Fukuda et al., 2003). Therefore, long-term disuse may result in the formation of myofibrils with expanded lattice spacing, due to preferential titin loss and ensuing defects in lattice stabilization. Our small-angle X-ray experiments indeed revealed that lattice spacing was expanded in disused fibers (by ~6% compared with control muscle) (Fig. 4 A). This finding was supported by an electron microscopy observation that revealed that the thick filament density was ~15% lower in disused fibers (Fig. 4 B). Osmotic compression of disused muscle with 2% (wt/vol) dextran T-500 (Dx; molecular weight, ~500,000) reduced lattice spacing to a similar level as observed in control muscle (Fig. 4 A), and completely restored Ca^{2+} sensitivity (Fig. 4 C). We therefore concluded that the expansion of lattice spacing is primarily responsible for the reduction in Ca^{2+} sensitivity (Fig. 2 A) (and, presumably, Ca^{2+}-independent active force; Fig. 2 B) in disused muscle via reduced cross-bridge formation.

However, Dx failed to restore maximal Ca^{2+}-activated force completely, where it was still lower by ~20% in disused muscle than in control muscle, in the presence of Dx (Fig. 4 C). Given the present findings that the

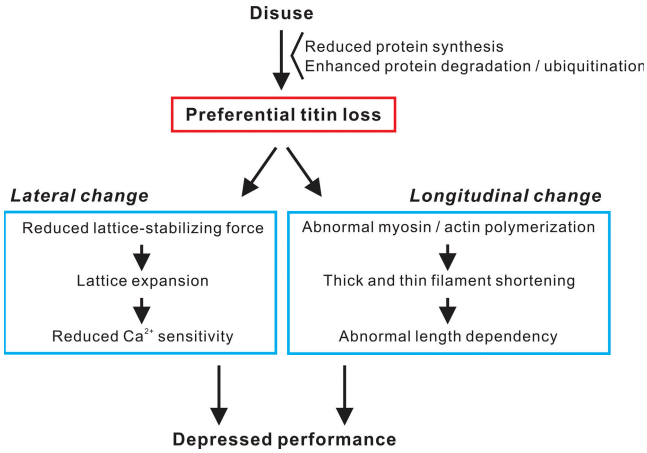

Figure 5. Flow chart showing the effects of disuse on skeletal muscle structure and function. Titin level is preferentially reduced in long-term disuse, via reduced synthesis and/or enhanced degradation (and/or ubiquitination), resulting in the formation of myofibrils with abnormal sarcomere structure, both laterally and longitudinally, thereby depressing muscle performance.

thick filament length is shorter by 0.05−0.1 μm (Fig. 1, C and D) and the thin filament length by ∼0.1 μm (Fig. 1 D) in the disused sarcomere, the shortening of thick and thin filaments (i.e., totally ∼20% reduction in the filament overlap at the full overlap state) can well account for the difference in maximal force between control and disused muscles, at a similar level of lattice spacing.

In conclusion, we demonstrated that preferential titin loss occurs in skeletal muscle in long-term disuse, associated with abnormal sarcomeric structure, in both longitudinal and lateral directions (Fig. 5). It is likely that the former results from abnormal myosin polymerization (and its secondary effect on thin filament length regulation) and the later from defects in lattice stabilization, both caused by the preferentially reduced titin level in disuse. The present work provides strong evidence that the longitudinal change accounts for the altered length dependence of active force and the lateral change underlies the reduced Ca^{2+} sensitivity, with overall depressions in active force production occurring synergistically due to these abnormalities in sarcomeric ultrastructure. Titin loss, namely, a reduction in PF, as well as depressed contractile force, is likely to induce unloading on the thick filament in the M-line region, which may progressively exacerbate sarcomeric integration via reduced titin kinase activation and the resultant reduction in muscle protein expression (Lange et al., 2005). Future studies should be directed to elucidating the transduction pathway(s) leading to preferential titin loss under various wasting conditions, aiming at developing novel pharmacological interventions that suppress muscle weakness by preventing disuse-induced defects in sarcomeric organization.

We thank Dr. Henk L. Granzier and Dr. Sergey V. Mikhailenko for critical reading of the manuscript. We also thank Ms. Naoko Tomizawa for technical support and Dr. Maki Yamaguchi for assistance with small-angle X-ray studies.

This study was supported in part by Grants-in-Aid for Scientific Research from the Ministry of Education, Culture, Sports, Science, and Technology of Japan and by grants from the Japan Science and Technology Agency (CREST), Mitsubishi Pharma Research Foundation, and Japan Cardiovascular Research Foundation to N. Fukuda.

Olaf S. Andersen served as editor.

Submitted: 20 September 2007
Accepted: 10 December 2007

REFERENCES

Cazorla, O., Y. Wu, T.C. Irving, and H. Granzier. 2001. Titin-based modulation of calcium sensitivity of active tension in mouse skinned cardiac myocytes. *Circ. Res.* 88:1028–1035.

Fitts, R.H., D.R. Riley, and J.J. Widrick. 2000. Physiology of a microgravity environment invited review: microgravity and skeletal muscle. *J. Appl. Physiol.* 89:823–839.

Fujita, H., K. Yasuda, S. Niitsu, T. Funatsu, and S. Ishiwata. 1996. Structural and functional reconstitution of thin filaments in the contractile apparatus of cardiac muscle. *Biophys. J.* 71:2307–2318.

Fukuda, N., H. Kajiwara, S. Ishiwata, and S. Kurihara. 2000. Effects of MgADP on length dependence of tension generation in skinned rat cardiac muscle. *Circ. Res.* 86:E1–E6.

Fukuda, N., D. Sasaki, S. Ishiwata, and S. Kurihara. 2001a. Length dependence of tension generation in rat skinned cardiac muscle: role of titin in the Frank-Starling mechanism of the heart. *Circulation.* 104:1639–1645.

Fukuda, N., J. O-Uchi, D. Sasaki, H. Kajiwara, S. Ishiwata, and S. Kurihara. 2001b. Acidosis or inorganic phosphate enhances the length dependence of tension in rat skinned cardiac muscle. *J. Physiol.* 536:153-160.

Fukuda, N., Y. Wu, T.C. Irving, and H. Granzier. 2003. Titin isoform variance and length dependence of activation in skinned bovine cardiac muscle. *J. Physiol.* 553:147–154.

Fukuda, N., Y. Wu, P. Nair, and H.L. Granzier. 2005. Phosphorylation of titin modulates passive stiffness of cardiac muscle in a titin isoform-dependent manner. *J. Gen. Physiol.* 125:257–271.

Glass, D.J. 2003. Signalling pathways that mediate skeletal muscle hypertrophy and atrophy. *Nat. Cell Biol.* 5:87–90.

Goto, K., R. Okuyama, M. Honda, H. Uchida, T. Akema, Y. Ohira, and T. Yoshioka. 2003. Profiles of connectin (titin) in atrophied soleus muscle induced by unloading of rats. *J. Appl. Physiol.* 94:897–902.

Granzier, H., and S. Labeit. 2004. The giant protein titin: a major player in myocardial mechanics, signaling, and disease. *Circ. Res.* 94:284–295.

Granzier, H.L., and T.C. Irving. 1995. Passive tension in cardiac muscle: contribution of collagen, titin, microtubules, and intermediate filaments. *Biophys. J.* 68:1027–1044.

Gregorio, C.C., H. Granzier, H. Sorimachi, and S. Labeit. 1999. Muscle assembly: a titanic achievement? *Curr. Opin. Cell Biol.* 11:18–25.

Helmes, M., K. Trombitas, and H. Granzier. 1996. Titin develops restoring force in rat cardiac myocytes. *Circ. Res.* 79:619–626.

Herzog, W., S. Kamal, and H.D. Clarke. 1992. Myofilament lengths of cat skeletal muscle: theoretical considerations and functional implications. *J. Biomech.* 25:945–948.

Higuchi, H., and Y. Umazume. 1986. Lattice shrinkage with increasing resting tension in stretched, single skinned fibers of frog muscle. *Biophys. J.* 50:385–389.

Ishiwata, S., K. Kinosita Jr., H. Yoshimura, and A. Ikegami. 1987. Rotational motions of myosin heads in myofibril studied by phosphorescence anisotropy decay measurements. *J. Biol. Chem.* 262:8314–8317.

Jackman, R.W., and S.C. Kandarian. 2004. The molecular basis of skeletal muscle atrophy. *Am. J. Physiol. Cell Physiol.* 287: C834–C843.

Lange, S., F. Xiang, A. Yakovenko, A. Vihola, P. Hackman, E. Rostkova, J. Kristensen, B. Brandmeier, G. Franzen, B. Hedberg, et al. 2005. The kinase domain of titin controls muscle gene expression and protein turnover. *Science.* 308:1599–1603.

Littlefield, R., and V.M. Fowler. 1998. Defining actin filament length in striated muscle: rulers and caps or dynamic stability? *Annu. Rev. Cell Dev. Biol.* 14:487–525.

Lynch, G.S., J.D. Schertzer, and J.G. Ryall. 2006. Therapeutic approaches for muscle wasting disorders. *Pharmacol. Ther.* 113:461–487.

McCormick, K.M., K.M. Baldwin, and A.F. Schachat. 1994. Coordinate changes in C protein and myosin expression during skeletal muscle hypertrophy. *Am. J. Physiol.* 267:C443–C449.

Mio, Y., N. Fukuda, Y. Kusakari, Y. Tanifuji, and S. Kurihara. 2002. Bupivacaine attenuates contractility by decreasing sensitivity of myofilaments to Ca^{2+} in rat ventricular muscle. *Anesthesiology.* 97:1168–1177.

Riley, D.A., J.L.W. Bain, J.L. Thompson, R.H. Fitts, J.J. Widrick, S.W. Trappe, T.A. Trappe, and D.L. Costill. 1998. Disproportionate loss of thin filaments in human soleus muscle after 17-day bed rest. *Muscle Nerve.* 21:1280–1289.

Riley, D.A., J.L.W. Bain, J.L. Thompson, R.H. Fitts, J.J. Widrick, S.W. Trappe, T.A. Trappe, and D.L. Costill. 2000. Decreased thin filament density and length in human atrophic soleus muscle fibers after spaceflight. *J. Appl. Physiol.* 88:567–572.

St-Amand, J., K. Okamura, K. Matsumoto, S. Shimizu, and Y. Sogawa. 2001. Characterization of control and immobilized skeletal muscle: an overview from genetic engineering. *FASEB J.* 15:684–692.

Toursel, T., L. Stevens, H. Granzier, and Y. Mounier. 2002. Passive tension of rat skeletal soleus muscle fibers: effects of unloading conditions. *J. Appl. Physiol.* 92:1465–1472.

Trinick, J. 1994. Titin and nebulin: protein rulers in muscle? *Trends Biochem. Sci.* 19:405–409.

van der Ven, P.F., J.W. Batsch, M. Gautel, H. Jockusch, and D.O. Furst. 2000. A functional knock-out of titin results in defective myofibril assembly. *J. Cell Sci.* 113:1405–1414.

Whiting, A., J. Wardale, and J. Trinick. 1989. Does titin regulate the length of muscle thick filaments? *J. Mol. Biol.* 205:263–268.

Yasuda, K., H. Fujita, Y. Fujiki, and S. Ishiwata. 1994. Length regulation of thin filaments without nebulin. *Proc. Jpn. Acad.* 70:151–156.